Experimental Quantum State Measurement with Classical Shadows

Zhang, Ting; Sun, Jinzhao; Fang, Xiao-Xu; Zhang, Xiao-Ming; Yuan, Xiao; Lu, He

Published in:
Physical Review Letters

Published: 12/11/2021

Document Version:
Final Published version, also known as Publisher's PDF, Publisher's Final version or Version of Record

Published version (DOI):
10.1103/PhysRevLett.127.200501

Publication details:
Zhang, T., Sun, J., Fang, X.-X., Zhang, X.-M., Yuan, X., & Lu, H. (2021). Experimental Quantum State Measurement with Classical Shadows. *Physical Review Letters*, *127*(20), Article 200501. https://doi.org/10.1103/PhysRevLett.127.200501

Zhang, T., Sun, J., Fang, X.-X., Zhang, X.-M., Yuan, X., & Lu, H. (2021). Experimental Quantum State Measurement with Classical Shadows. *Physical Review Letters, 127(*20), Article 200501. https://doi.org/10.1103/PhysRevLett.127.200501

Experimental Quantum State Measurement with Classical Shadows

Ting Zhang,[1,*] Jinzhao Sun,[2,3,*] Xiao-Xu Fang,[1] Xiao-Ming Zhang,[2,4] Xiao Yuan,[2,†] and He Lu[1,‡]
[1]School of Physics, Shandong University, Jinan 250100, China
[2]Center on Frontiers of Computing Studies, Peking University, Beijing 100871, China
[3]Clarendon Laboratory, University of Oxford, Parks Road, Oxford OX1 3PU, United Kingdom
[4]Department of Physics, City University of Hong Kong, Tat Chee Avenue, Kowloon, Hong Kong SAR, China

(Received 5 July 2021; accepted 30 September 2021; published 8 November 2021)

A crucial subroutine for various quantum computing and communication algorithms is to efficiently extract different classical properties of quantum states. In a notable recent theoretical work by Huang, Kueng, and Preskill [Nat. Phys. **16**, 1050 (2020)], a thrifty scheme showed how to project the quantum state into classical shadows and simultaneously predict M different functions of a state with only $\mathcal{O}(\log_2 M)$ measurements, independent of the system size and saturating the information-theoretical limit. Here, we experimentally explore the feasibility of the scheme in the realistic scenario with a finite number of measurements and noisy operations. We prepare a four-qubit GHZ state and show how to estimate expectation values of multiple observables and Hamiltonians. We compare the measurement strategies with uniform, biased, and derandomized classical shadows to conventional ones that sequentially measure each state function exploiting either importance sampling or observable grouping. We next demonstrate the estimation of nonlinear functions using classical shadows and analyze the entanglement of the prepared quantum state. Our experiment verifies the efficacy of exploiting (derandomized) classical shadows and sheds light on efficient quantum computing with noisy intermediate-scale quantum hardware.

DOI: 10.1103/PhysRevLett.127.200501

Quantum computers could process information in parallel and efficiently represent many-body quantum states [1–4]. Yet, the power of quantum computing is subject to how efficiently we extract classical information from the quantum state. Focusing on variational quantum algorithms designed for near-term quantum devices [1–17], whether they are sufficiently effective to demonstrate clear and robust quantum advantages, relies on how efficiently we can measure the state [7,18–30]. For example, the Hamiltonian of a molecule with M modes has $\mathcal{O}(M^4)$ terms and a naive strategy requires $\mathcal{O}(M^8/\varepsilon^2)$ samples to measure each term to an accuracy ε [1,11,31]. In order to demonstrate a quantum advantage, we need to consider a sufficiently large M, say 100, and the cost of naively measuring those quantum systems could already be impractically large.

Advanced measurement schemes have been proposed to more efficiently evaluate observable expectation values without increasing the circuit depth [28–30,32–40]. One can use the strategy of importance sampling to economically distribute more measurements to observables with large contributions [18,35], or group compatible observables to reduce the cost in estimating low-weight qubit reduced density matrices [39,40] or observable expectations [9,24,25,32,33,41].

Another notable scheme [34,42–49] shows how to simultaneously obtain expectation values of multiple observables by randomly measuring and projecting the quantum state into classical shadows (CS). The algorithm only requires $\mathcal{O}(\log_2 M)$ samples to measure M low-weight observables, and the recently proposed locally biased CS [36] and derandomized CS [37] can be further applied to general observables with numerical results showing advantages over most other existing methods.

While the advanced measurement schemes have been extensively studied in theory, their feasibility and comparison with realistic hardware are under exploration. In particular, efficiently implementing random measurements and analyzing how the noise in realistic hardware affects the measurement efficiency are critical for studying their practical performance with realistic devices.

Here, we experimentally investigate the feasibility of the advanced measurement schemes with a four-qubit photonic quantum processor. We consider the schemes using importance sampling [18,35], observable grouping [32,33,41], and the three schemes with uniformly random [34], biased random [36], and derandomized [37] classical shadows in tasks of estimating multiple local observables and computing the expectation of the Hamiltonian and its powers. We further apply the classical shadows to estimate the state purity and moments of the partially transposed density matrix, which helps to analyze its entanglement structure [50]. Our experimental results clearly show advantages of using (derandomized) classical shadows with realistic quantum devices.

Framework.—We first review the advanced measurement schemes in a unified framework recently proposed in Ref. [51]. We aim to estimate the expectation value of an observable $\mathbf{O}$, which is decomposed into the Pauli basis as $\mathbf{O} = \sum_l \alpha_l \mathbf{O}_l$, with $\mathbf{O}_l \in \{I, X, Y, Z\}^{\otimes n}$ being the tensor product of single-qubit Pauli operators. For a multiqubit Pauli operator $\mathbf{Q} = \otimes_{i=1}^n Q_i$ with $Q_i \in \{I, X, Y, Z\}$ being a single-qubit Pauli operator acting on the ith qubit, its expectation value can be obtained by measurements in any Pauli basis $\mathbf{P} = \otimes_{i=1}^n P_i$, whenever $Q_i = P_i$ or $Q_i = I$ for any i, which we refer to as $\mathbf{P}$ hits $\mathbf{Q}$ and denote by $\mathbf{Q} \triangleright \mathbf{P}$. When two Pauli observables are hit by the same basis $\mathbf{P}$, we say that they are compatible with each other, and their expectation values can be simultaneously obtained by measuring the basis $\mathbf{P}$. Considering two extreme cases of measuring $\mathbf{O} = \sum_l \alpha_l \mathbf{O}_l$, the first one is that all the expectation values of $\mathbf{O}_l$ can be determined by one measurement $\mathbf{P}$ if $\mathbf{O}_l \triangleright \mathbf{P}$ ($\forall\, l$), i.e., every $\mathbf{O}_l$ is compatible with each other. On the contrary, we have to measure every $\mathbf{O}_l$ if no observable is compatible with any other one.

In general, to estimate $\mathrm{Tr}(\rho \mathbf{O})$ for an n-qubit unknown quantum state ρ, the measurement $\mathbf{P}$ is randomly selected over the distribution $\mathcal{K}(\mathbf{P})$. An estimator for the target observable $\mathbf{O}$ is expressed as

$$\hat{\mathbf{o}}(\mathbf{P}) = \sum_l \alpha_l f(\mathbf{P}, \mathbf{O}_l, \mathcal{K}) \mu[\mathbf{P}, \mathrm{supp}(\mathbf{O}_l)], \tag{1}$$

where $\mu[\mathbf{P}, \mathrm{supp}(\mathbf{O}_l)] = \prod_{i \in \mathrm{supp}(\mathbf{O}_l)} \mu(P_i)$ with $\mu(P_i)$ being the single-shot outcome of measurement P_i on the ith qubit, $\mathrm{supp}(\mathbf{Q}) = \{i | Q_i \neq I\}$, and the function f depends on the measurement scheme. For different measurement schemes, we show in the following different choices of $\mathcal{K}(\mathbf{P})$ and the function f that give an unbiased estimation

$$\mathbb{E}[\hat{\mathbf{o}}] = \mathrm{Tr}(\mathbf{O}\rho), \tag{2}$$

where the average is over $\mathcal{K}(\mathbf{P})$.

An importance sampling method [35], which is also called l_1 sampling, corresponds to the case with $\mathbf{P}_l = \mathbf{O}_l$, $\mathcal{K}(\mathbf{P}_l) = |\alpha_l| / \sum_l |\alpha_l|$, and $f(\mathbf{P}, \mathbf{O}_l, \mathcal{K}) = \mathcal{K}(\mathbf{P})^{-1} \delta_{\mathbf{P}, \mathbf{O}_l}$. Heuristic grouping methods, such as the one using the largest degree first (LDF) grouping [32,33,41], divide $\mathcal{O} = \{\mathbf{O}_l\}$ into several groups $\mathcal{S}_j$ such that $\cup_j \mathcal{S}_j = \mathcal{O}$, $\mathcal{S}_j \cap \mathcal{S}_{j'} = \varnothing$, $\forall\ j \neq j'$. For each group $\mathcal{S}_j$, measurement $\mathbf{P}_j$ is assigned such that $\mathbf{Q} \triangleright \mathbf{P}_j$, $\forall\ \mathbf{Q} \in \mathcal{S}_j$ with probabilities $\mathcal{K}(\mathbf{P}_j)$ chosen either uniformly or based on the total weight of the observables in the set $\mathbf{P}_j$. The function is chosen as $f(\mathbf{P}_j, \mathbf{Q}, \mathcal{K}) = \mathcal{K}(\mathbf{P}_j)^{-1} \delta_{\mathbf{Q} \in \mathcal{S}_j}$. Although finding the optimal grouping strategy is NP hard in decomposition of the complex Hamiltonian, the heuristic grouping methods could give suboptimal strategies, especially for the Hamiltonian containing many compatible terms [33].

The conventional classical shadow (CS) method [34] considers the full-weight Pauli basis set $\mathbf{P} \in \{X, Y, Z\}^{\otimes n}$ with a uniform probability $\mathcal{K}(\mathbf{P}) = 1/3^n$. One of its generalization is to consider locally biased classical shadow (LBCS) [36] with product and biased probability $\mathcal{K}(\mathbf{P}) = \prod_i \mathcal{K}_i(P_i)$, where $\mathcal{K}_i(P_i)$ represents the probability of measuring the ith site with the basis P_i. For the CS and LBCS methods, the function is defined as $f(\mathbf{P}, \mathbf{Q}, \mathcal{K}) = \prod_i f_i(P_i, Q_i, \mathcal{K}_i)$ with $f_i(P_i, Q_i, \mathcal{K}_i) = \delta_{Q_i, I_2} + \mathcal{K}_i(P_i)^{-1} \delta_{Q_i, P_i}$. Huang *et al.* further proposed the derandomized shadow method, in which the basis set is deterministically chosen by a classical greedy algorithm [37]. For the CS methods, the randomized measurement is implemented by applying random local Clifford unitaries. Besides the estimation of expected values of observables, we can also use classical shadows to calculate nonlinear properties of quantum states, in particular observables of higher state moments, as suggested in Refs. [34,52–54]. We refer to the Supplemental Material [55] for detailed discussions on the implementation of the CS scheme and the measurement cost complexity.

Prior experiments have implemented the original CS method using uniform probability distribution. In particular, Struchalin *et al.* [43] demonstrated the estimation of local observables and the state fidelity with uniformly random stablizer measurements on an optical system, and Elben *et al.* [52] used prior experimental data of trapped ions from randomized measurements to detect the bipartite entanglement. Here we focus on all the latest CS methods and compare them to other advanced measurement schemes. We consider the tasks of measuring linear and nonlinear observables and show the application and advantage of using classical shadows.

Experimental setup.—We implement the advanced measurement schemes on a photonic four-qubit Greenberger-Horne-Zeilinger (GHZ) state with ideal form of $|\mathrm{GHZ}_4\rangle = (|0000\rangle + |1111\rangle)/\sqrt{2}$. As shown in Fig. 1(a), the polarization-entangled photons are generated from a periodically poled potassium titanyl phosphate (PPKTP) crystal in a Sagnac interferometer [60], which is bidirectionally pumped by an ultraviolet (UV) laser diode with central wavelength of 405 nm. The two photons are entangled in the polarization degree of freedom (DOF) with ideal form of $|\Phi^+\rangle = (|HH\rangle + |VV\rangle)/\sqrt{2}$, where $|H\rangle$ and $|V\rangle$ denote horizontal and vertical polarization, respectively. Each photon is then extended to its path DOF by passing through a beam displacer (BD) which transmits vertical component and deviates horizontal component. Thus, a four-qubit hyperentangled state $|\mathrm{GHZ}_4\rangle = (|HhHh\rangle + |VvVv\rangle)/\sqrt{2}$ is generated, where h and v denote the path DOF. The qubit is encoded in the polarization DOF as $|H(V)\rangle \to |0(1)\rangle$, and in the path DOF as $|h(v)\rangle \to |0(1)\rangle$ [61]. The measurements on basis $\mathbf{P}$ on polarization DOF and path DOF are realized with setups shown in Fig. 1(c). The single-qubit Clifford unitaries on either polarization or path DOF

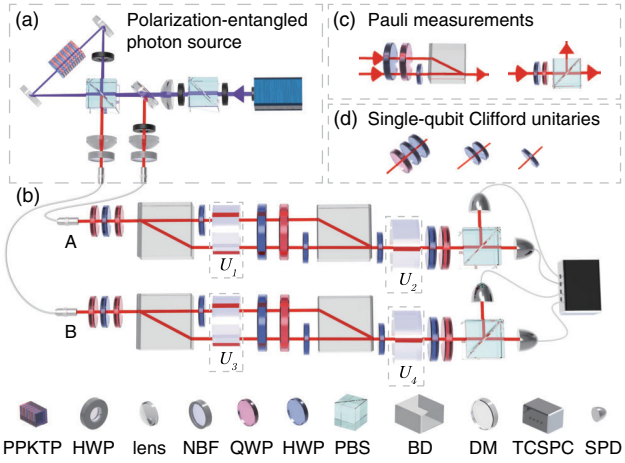

FIG. 1. Schematic illustration of the experimental setup. (a) The setup to generate maximally polarization-entangled photon pair. (b) Two photons are sent into BD to generate a four-qubit hyperentangled state. (c) Experimental setup to implement the Pauli measurements. (d) The single-qubit Clifford operations (U_i) are realized with different settings of wave plates. Narrow-band filter (NBF); Dichroic mirror (DM).

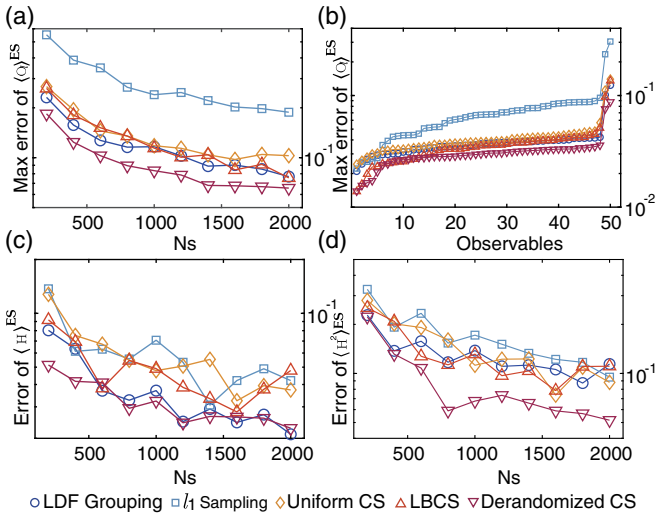

FIG. 2. The error of observable estimations with five different measurement schemes. (a) The maximum absolute error of $\langle \mathbf{O}_l \rangle^{\mathrm{ES}}$ over 50 local observables $\mathbf{O}_l$ that are randomly selected from the Pauli set with different number of N_s. (b) The maximum absolute error of $\langle \mathbf{O}_l \rangle^{\mathrm{ES}}$ with different number of local observables, each of which we fix $N_s = 2000$. (c) and (d) Errors of estimated energy $\langle H \rangle^{\mathrm{ES}}$ and that of estimated Hamiltonian moment $\langle H^2 \rangle^{\mathrm{ES}}$ with different N_s. In each measurement basis we collect five coincidences for data processing, and we run 20 independent repetitions of the entire setup.

are realized by sets of half-wave plate (HWP) and quarter-wave plate (QWP) as shown in Fig. 1(d). All the photons are collected with single-mode fibres and detected by single-photon detectors (SPD). The arriving time (time tag) of each photon is recorded by a time-correlated single-photon counting (TCSPC) system. By counting the time tags, the coincidence (as low as 1) on each measurement basis can be determined, as well as its corresponding statistical time. We implement the quantum state tomography (QST) on the prepared state $\rho_{\mathrm{exp}}^{\mathrm{GHZ}_4}$, and calculate that the fidelity of $\rho_{\mathrm{exp}}^{\mathrm{GHZ}_4}$ and $|\mathrm{GHZ}_4\rangle$ is $\mathcal{F} = 0.9546 \pm 0.0006$. We refer to Ref. [55] for more details of experimental demonstrations and data processing.

Estimation of observables.—We perform the classical shadow (CS) schemes (uniform CS, locally biased CS, and derandmized CS) as well as conventional schemes (l_1 sampling and LDF grouping) on the prepared state $\rho_{\mathrm{exp}}^{\mathrm{GHZ}_4}$. We randomly select 50 observables $\mathbf{O}_l$ ($l \leq 50$) that are tensor products of Pauli operators acting nontrivially on maximally two qubits. The measurement bases are determined according to the target observables and the measurement scheme. Experimentally, the estimation is determined with the results from N_s measurements (also called samples), in each of which we collect five coincidences. We postprocess the measurement results using Eq. (1) to estimate the expectation value of target observables. The maximal errors of estimated expectation $\langle \mathbf{O}_l \rangle^{\mathrm{ES}}$ over 50 Pauli observables $\mathbf{O}_l$ with five estimation schemes are shown in Fig. 2, where the error is defined as the difference between $\langle \mathbf{O}_l \rangle^{\mathrm{ES}}$ and results with direct measurement of $\mathbf{O}_l$ on $\rho_{\mathrm{exp}}^{\mathrm{GHZ}_4}$. In Fig. 2(a), we observe that the maximal error of $\langle \mathbf{O}_l \rangle^{\mathrm{ES}}$ decreases with an increasing number of measurements N_s. Except for l_1 sampling, we observe the maximum error is reduced to 0.1 when $N_s = 2000$. Next, we fix N_s and investigate the maximal error with an increasing number of observables, and the results are shown in Fig. 2(b). We observe that the accuracy with the derandomized CS method outperforms those with other schemes, especially the l_1 sampling method.

Moreover, we demonstrate the estimation of energy and Hamiltonian moment in the variational quantum simulation [2,62–64]. We consider the Hamiltonian in the form of $H = J\sum_i (Z_iZ_{i+1} + X_iY_{i+1} + Y_iZ_{i+1} + X_iZ_{i+1}) + h\sum_i X_i$ with the periodic boundary condition. The results for $\langle H \rangle^{\mathrm{ES}}$ and its second-order moments $\langle H^2 \rangle^{\mathrm{ES}}$ with normalized strength $J = h = 1/4$ are shown in Fig. 2(c) and Fig. 2(d), respectively. Similarly, the error decreases with an increasing of N_s. We also observe that the results with LDF grouping and derandomized CS schemes outperform other schemes for the energy estimation as shown in Fig. 2(c), while derandomized CS shows significant advantage in the estimation of $\langle H^2 \rangle^{\mathrm{ES}}$ as reflected in Fig. 2(d) owing to many large-support terms in H^2. One can expect that the advanced measurement schemes could be more competitive when the problem size increases. We leave the discussion on statistical errors, numerical simulations with noiseless state, noise robustness, and results for cluster Hamiltonian with Ising interactions and the hydrogen molecular Hamiltonian to the Supplemental Material [55].

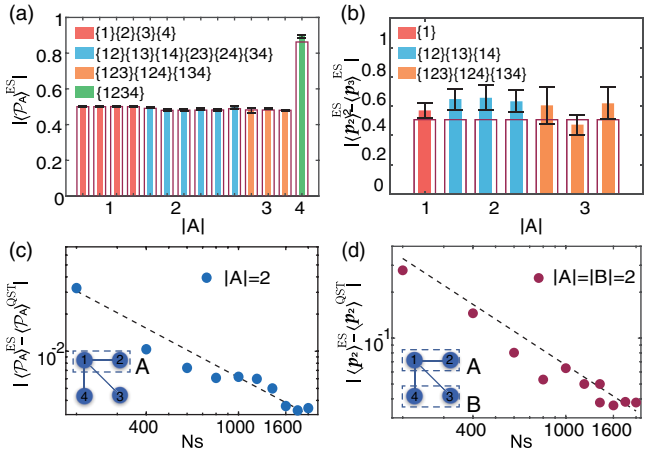

FIG. 3. Experimental results for estimating nonlinear functions with classical shadows. (a) The estimation of subsystem purity $\langle \mathcal{P}_A \rangle^{\mathrm{ES}}$ with the different subsystems A. The colored bars represent the results from the CS method, while the red sticks represent the results from QST for comparison. (b) The estimation of $p_2^2 - p_3$ for different subsystem partitioning of the prepared GHZ state, which clearly shows the violation of the p_3-PPT condition. The number of measurements N_s in (a) and (b) is fixed as 1000 for the CS method, and the standard deviation is obtained by repeating the experiment 10 times. Here, we collect one coincidence at each measurement. The dots in (c) and (d) represent the errors of $\langle \mathcal{P}_A \rangle^{\mathrm{ES}}$ and that of $\langle p_2 \rangle^{\mathrm{ES}}$ with different N_s, respectively. The dashed line represents the scaling of $\propto 1/N_s$. The $|\mathrm{GHZ}_4\rangle$ is a specific graph state, corresponding to a star graph, which is exhibited in the insets.

Estimation of nonlinear function and entanglement structure.—We divide the four-qubit GHZ state $\rho_{\mathrm{exp}}^{\mathrm{GHZ}_4}$ into two subsystems A and B, where B is the complement set ($A \cup B = \{1,2,3,4\}$ and $A \cap B = \varnothing$). Each subsystem contains $|A|$ and $|B|$ qubits, respectively. The purity of subsystem A can be measured on two copies of ρ_A by $\mathcal{P}_A = \mathrm{Tr}[\rho_A^2] = \mathrm{Tr}[\Pi_A \rho \otimes \rho]$, where Π_A is the local swap operator of two copies of the subsystem A [65,66]. Instead, we can make use of the classical shadows to predict the expectation of high-order target functions. The classical shadows of the underlying state ρ can be generated by applying single-qubit Clifford unitary U_i on the ith qubit drawn from a uniformly random distribution and collecting its corresponding outcome $|\mathbf{b}_i\rangle$ from projective measurements. The unbiased estimator $\hat{\rho}$ is given by $\hat{\rho} = \bigotimes_i (3U_i^\dagger |\mathbf{b}_i\rangle\langle \mathbf{b}_i| U_i - I_2)$, and $\mathbb{E}[\hat{\rho}] = \rho$ (More details can be found in Ref. [55]). Note that the estimator of the subsystem state A can be generated by choosing the index of qubit $i \in A$. In experiment, we generated $N_s = 1000$ independent classical shadows $\hat{\rho}_A^{(k)}$ obtained from measurements on the prepared state under uniformly random local Clifford unitaries. Then, we randomly select two independent $\hat{\rho}_A^{(k_1)}$ and $\hat{\rho}_A^{(k_2)}$, and estimate the subsystem purity by $\hat{\mathcal{P}}_A = \sum_{k_1 \neq k_2} \mathrm{Tr}[\hat{\rho}_A^{(k_1)} \otimes \hat{\rho}_A^{(k_2)}]/N_s(N_s - 1)$. Here, we improve the estimation accuracy by exploiting all the distinct samples [34,52,67]. Figure 3(a) shows the estimation results for the subsystem purity estimation $\mathcal{P}_A$ for all possible divisions of subsystems. We observe that $\langle \mathcal{P}_A \rangle^{\mathrm{ES}} < \langle \mathcal{P}_{AB} \rangle^{\mathrm{ES}}$ for all the subsystems $A \subseteq \{1,2,3,4\}$, which certifies genuine multipartite entanglement of the prepared state [65].

We next demonstrate another entanglement detection based on the positive partial transpose (PPT) condition, which checks whether the partially transposed (PT) density matrix $\rho_{AB}^{T_A}$ has negative eigenvalues. We consider the PT moments $p_n = \mathrm{Tr}[(\rho_{AB}^{T_A})^n]$, and it has been shown that the state must be entangled if $p_2^2 > p_3$ [52,53]. Note that $\mathrm{Tr}[(\rho_{AB}^{T_A})^n] = \mathrm{Tr}[\vec{\Pi}_A \overleftarrow{\Pi}_B \rho_{AB}^{\otimes n}]$, where $\vec{\Pi}_A$ and $\overleftarrow{\Pi}_B$ are n-copy cyclic permutation operators that act on the subsystems A and B, respectively. The typical procedure to estimate p_n requires measuring the observable $\vec{\Pi}_A \overleftarrow{\Pi}_B$ on n copies of quantum states. Instead, we can construct the U-statistic estimator of p_n by summing over all possible pairs of the independent classical shadows [53]: $\hat{p}_n = \{1/[n!\binom{N_s}{n}]\} \sum_{k_1 \neq \cdots \neq k_n} \mathrm{Tr}[\vec{\Pi}_A \overleftarrow{\Pi}_B \hat{\rho}_{AB}^{(k_1)} \otimes \cdots \otimes \hat{\rho}_{AB}^{(k_n)}]$, and the estimator is unbiased as $\mathbb{E}[\hat{p}_n] = p_n$. The PT moment can be efficiently computed as the summands are tensor products of local density matrix and is complete to factorize into contractions of single-qubit matrices [52]. The estimation of $|(\langle p_2 \rangle^{\mathrm{ES}})^2 - \langle p_3 \rangle^{\mathrm{ES}}|$ for different subsystem divisions are shown in Fig. 3(b) which clearly violates the p_3-PPT condition ($p_2^2 > p_3$) and indicates the genuine bipartite entanglement of the prepared state. Compared to the purity condition [$\mathrm{Tr}(\rho_A^2) < \mathrm{Tr}(\rho_{AB}^2)$], p_3-PPT condition can be applied to detect entanglement of mixed state [52], and more details can be found in Ref. [55].

The estimation errors of subsystem purity $|\langle \mathcal{P}_A \rangle^{\mathrm{ES}} - \langle \mathcal{P}_A \rangle^{\mathrm{QST}}|$ and the PT moment $|\langle p_2 \rangle^{\mathrm{ES}} - \langle p_2 \rangle^{\mathrm{QST}}|$ of the case $A = \{1,2\}$ and $B = \{3,4\}$ are shown in Fig. 3(c) and Fig. 3(d), respectively, where $\langle \bullet \rangle^{\mathrm{QST}}$ is the results calculated with reconstructed $\rho_{\mathrm{exp}}^{\mathrm{GHZ}_4}$ from quantum state tomography. Similarly, we observe that the estimation can be inferred using a small number of N_s and becomes more accurate when N_s increases. The estimation error decays proportionally to $1/N_s$ for a small number of samples, different from the asymptotic decay rate in the large sample limit. We also discuss the sample complexity for estimating general nonlinear function in the Supplemental Material [55].

Conclusion.—In this work, we experimentally study the feasibility of quantum measurements. We compare the advanced measurement schemes with no increase in the circuit depth, and show that the (derandomized) classical shadow method outperforms other advanced measurement schemes, especially the naive l_1 sampling measurement method, in estimating linear observables, and it applies to extract the nonlinear functions of states. While we demonstrate the measurement on a small quantum device, these measurement schemes works naturally for problems with larger sizes. Since the Hamiltonian of

a larger problem could be even more complicated, the advanced measurement schemes could hence show more advantages in reducing the measurement cost. Several other measurement schemes were posted very recently [47,48,51], which improve the energy estimation by introducing optimized measurement schemes within the unified framework. The only difference is the selection of the measurement basis, and thus one can similarly compare those measurement schemes by experiments. Also, we experimentally demonstrate that the classical shadow method applies to the estimation of Hamiltonian moments $\langle H^n \rangle$, which can be leveraged to correct the ground state energy obtained from the variational approach [63,64] or in the adaptive variational quantum algorithms [68–70]. Moreover, one could minimize the variance of eigenenergy $\langle H^2 \rangle - \langle H \rangle^2$ to prepare the excited states of H in the variational quantum simulation [62]. Those tasks generally require a prohibitively large number of measurements, which, however, could be significantly alleviated using classical shadows. We also demonstrate the detection of genuine entanglement using classical shadows, whose extension to general entanglement structure detection deserves future studies.

Our work verifies the possibility of efficient measurement of quantum states and paves the way for fast quantum processing using near-term quantum devices. One direction for further research is to incorporate error mitigation into the measurement schemes [3,71–76]. Error mitigation is able to suppress device errors, which leads the estimation to be more accurate compared to the ideal value. As the CS scheme could be robust to shot noise, the combination of these two schemes is expected to make the estimation with high accuracy as well as high confidence.

We thank Bujiao Wu and Vlatko Vedral for insightful discussions on the framework. This work is supported by the National Key R&D Program of China (Grant No. 2019YFA0308200), National Natural Science Foundation of China (Grants No. 11974213 and No. 92065112), Shandong Provincial Natural Science Foundation (Grants No. ZR2019MA001 and No. ZR2020JQ05), Taishan Scholar of Shandong Province (Grant No. tsqn202103013) and Shandong University Multidisciplinary Research and Innovation Team of Young Scholars (Grant No. 2020QNQT).

*These authors contributed equally to this work.
†xiaoyuan@pku.edu.cn
‡luhe@sdu.edu.cn

[1] S. McArdle, S. Endo, A. Aspuru-Guzik, S. C. Benjamin, and X. Yuan, Rev. Mod. Phys. **92**, 015003 (2020).
[2] M. Cerezo, A. Arrasmith, R. Babbush, S. C. Benjamin, S. Endo, K. Fujii, J. R. McClean, K. Mitarai, X. Yuan, L. Cincio, and P. J. Coles, Nat. Rev. Phys. **3**, 625 (2021).
[3] S. Endo, Z. Cai, S. C. Benjamin, and X. Yuan, J. Phys. Soc. Jpn. **90**, 032001 (2021).
[4] J. I. Colless, V. V. Ramasesh, D. Dahlen, M. S. Blok, M. E. Kimchi-Schwartz, J. R. McClean, J. Carter, W. A. de Jong, and I. Siddiqi, Phys. Rev. X **8**, 011021 (2018).
[5] A. Peruzzo, J. McClean, P. Shadbolt, M.-H. Yung, X.-Q. Zhou, P. J. Love, A. Aspuru-Guzik, and J. L. O'Brien, Nat. Commun. **5**, 4213 (2014).
[6] K. Bharti, A. Cervera-Lierta, T. H. Kyaw, T. Haug, S. Alperin-Lea, A. Anand, M. Degroote, H. Heimonen, J. S. Kottmann, T. Menke, W.-K. Mok, S. Sim, L.-C. Kwek, and A. Aspuru-Guzik, arXiv:2101.08448.
[7] W. J. Huggins, J. R. McClean, N. C. Rubin, Z. Jiang, N. Wiebe, K. B. Whaley, and R. Babbush, npj Quantum Inf. **7**, 23 (2021).
[8] S. Endo, J. Sun, Y. Li, S. C. Benjamin, and X. Yuan, Phys. Rev. Lett. **125**, 010501 (2020).
[9] C. Hempel, C. Maier, J. Romero, J. McClean, T. Monz, H. Shen, P. Jurcevic, B. P. Lanyon, P. Love, R. Babbush, A. Aspuru-Guzik, R. Blatt, and C. F. Roos, Phys. Rev. X **8**, 031022 (2018).
[10] X. Yuan, S. Endo, Q. Zhao, Y. Li, and S. C. Benjamin, Quantum **3**, 191 (2019).
[11] G. A. Quantum *et al.*, Science **369**, 1084 (2020).
[12] X. Yuan, J. Sun, J. Liu, Q. Zhao, and Y. Zhou, Phys. Rev. Lett. **127**, 040501 (2021).
[13] K. Fujii, K. Mitarai, W. Mizukami, and Y. O. Nakagawa, arXiv:2007.10917.
[14] B. Commeau, M. Cerezo, Z. Holmes, L. Cincio, P. J. Coles, and A. Sornborger, arXiv:2009.02559.
[15] C. Bravo-Prieto, R. LaRose, M. Cerezo, Y. Subasi, L. Cincio, and P. J. Coles, arXiv:1909.05820.
[16] X. Xu, J. Sun, S. Endo, Y. Li, S. C. Benjamin, and X. Yuan, Sci. Bull. **66**, 2181 (2021).
[17] H.-Y. Huang, K. Bharti, and P. Rebentrost, arXiv:1909.07344.
[18] J. R. McClean, J. Romero, R. Babbush, and A. Aspuru-Guzik, New J. Phys. **18**, 023023 (2016).
[19] Y. Cao, J. Romero, J. P. Olson, M. Degroote, P. D. Johnson, M. Kieferová, I. D. Kivlichan, T. Menke, B. Peropadre, N. P. D. Sawaya, S. Sim, L. Veis, and A. Aspuru-Guzik, Chem. Rev. **119**, 10856 (2019).
[20] A. F. Izmaylov, T.-C. Yen, and I. G. Ryabinkin, Chem. Sci. **10**, 3746 (2019).
[21] N. C. Rubin, R. Babbush, and J. McClean, New J. Phys. **20**, 053020 (2018).
[22] B. O'Gorman, W. J. Huggins, E. G. Rieffel, and K. B. Whaley, arXiv:1905.05118.
[23] T.-C. Yen, V. Verteletskyi, and A. F. Izmaylov, arXiv:1907.09386.
[24] A. F. Izmaylov, T.-C. Yen, R. A. Lang, and V. Verteletskyi, arXiv:1907.09040.
[25] A. Zhao, A. Tranter, W. M. Kirby, S. F. Ung, A. Miyake, and P. J. Love, Phys. Rev. A **101**, 062322 (2020).
[26] J. Sun, S. Endo, H. Lin, P. Hayden, V. Vedral, and X. Yuan, arXiv:2106.05938.
[27] P. Gokhale, O. Angiuli, Y. Ding, K. Gui, T. Tomesh, M. Suchara, M. Martonosi, and F. T. Chong, arXiv:1907.13623.
[28] G. Torlai, G. Mazzola, J. Carrasquilla, M. Troyer, R. Melko, and G. Carleo, Nat. Phys. **14**, 447 (2018).
[29] J. Carrasquilla, G. Torlai, R. G. Melko, and L. Aolita, Nat. Mach. Intell. **1**, 155 (2019).

[30] G. Torlai, G. Mazzola, G. Carleo, and A. Mezzacapo, Phys. Rev. Research **2**, 022060(R) (2020).
[31] R. Babbush, N. Wiebe, J. McClean, J. McClain, H. Neven, and G. K.-L. Chan, Phys. Rev. X **8**, 011044 (2018).
[32] A. Kandala, A. Mezzacapo, K. Temme, M. Takita, M. Brink, J. M. Chow, and J. M. Gambetta, Nature (London) **549**, 242 (2017).
[33] V. Verteletskyi, T.-C. Yen, and A. F. Izmaylov, J. Chem. Phys. **152**, 124114 (2020).
[34] H.-Y. Huang, R. Kueng, and J. Preskill, Nat. Phys. **16**, 1050 (2020).
[35] D. Wecker, M. B. Hastings, and M. Troyer, Phys. Rev. A **92**, 042303 (2015).
[36] C. Hadfield, S. Bravyi, R. Raymond, and A. Mezzacapo, arXiv:2006.15788.
[37] H.-Y. Huang, R. Kueng, and J. Preskill, Phys. Rev. Lett. **126**, 190505 (2021).
[38] K. Choo, A. Mezzacapo, and G. Carleo, Nat. Commun. **11**, 2368 (2020).
[39] X. Bonet-Monroig, R. Babbush, and T. E. O'Brien, Phys. Rev. X **10**, 031064 (2020).
[40] J. Cotler and F. Wilczek, Phys. Rev. Lett. **124**, 100401 (2020).
[41] P. J. J. O'Malley *et al.*, Phys. Rev. X **6**, 031007 (2016).
[42] S. Aaronson, SIAM J. Comput. **49**, STOC18-368 (2020).
[43] G. I. Struchalin, Y. A. Zagorovskii, E. Kovlakov, S. S. Straupe, and S. P. Kulik, PRX Quantum **2**, 010307 (2021).
[44] S. Chen, W. Yu, P. Zeng, and S. T. Flammia, PRX Quantum **2**, 030348 (2021).
[45] A. Zhao, N. C. Rubin, and A. Miyake, Phys. Rev. Lett. **127**, 110504 (2021).
[46] A. Acharya, S. Saha, and A. M. Sengupta, arXiv:2105.05992.
[47] C. Hadfield, arXiv:2105.12207.
[48] S. Hillmich, C. Hadfield, R. Raymond, A. Mezzacapo, and R. Wille, arXiv:2105.06932.
[49] R. J. Garcia, Y. Zhou, and A. Jaffe, Phys. Rev. Research **3**, 033155 (2021).
[50] H. Lu, Q. Zhao, Z.-D. Li, X.-F. Yin, X. Yuan, J.-C. Hung, L.-K. Chen, L. Li, N.-L. Liu, C.-Z. Peng, Y.-C. Liang, X. Ma, Y.-A. Chen, and J.-W. Pan, Phys. Rev. X **8**, 021072 (2018).
[51] B. Wu, J. Sun, Q. Huang, and X. Yuan, arXiv:2105.13091.
[52] A. Elben, R. Kueng, H.-Y. R. Huang, R. van Bijnen, C. Kokail, M. Dalmonte, P. Calabrese, B. Kraus, J. Preskill, P. Zoller, and B. Vermersch, Phys. Rev. Lett. **125**, 200501 (2020).
[53] A. Neven, J. Carrasco, V. Vitale, C. Kokail, A. Elben, M. Dalmonte, P. Calabrese, P. Zoller, B. Vermersch, R. Kueng, and B. Kraus, arXiv:2103.07443.
[54] V. Vitale, A. Elben, R. Kueng, A. Neven, J. Carrasco, B. Kraus, P. Zoller, P. Calabrese, B. Vermersch, and M. Dalmonte, arXiv:2101.07814.
[55] See Supplemental Material at http://link.aps.org/supplemental/10.1103/PhysRevLett.127.200501 for the framework, theoretical analysis, experimental implementations, and results, which includes Refs. [56–59].
[56] W. Son, L. Amico, R. Fazio, A. Hamma, S. Pascazio, and V. Vedral, Europhys. Lett. **95**, 50001 (2011).
[57] S. O. Skrøvseth and S. D. Bartlett, Phys. Rev. A **80**, 022316 (2009).
[58] Z. Webb, arXiv:1510.02769.
[59] J.-Y. Li, X.-X. Fang, T. Zhang, G. N. M. Tabia, H. Lu, and Y.-C. Liang, Phys. Rev. Research **3**, 023045 (2021).
[60] T. Kim, M. Fiorentino, and F. N. C. Wong, Phys. Rev. A **73**, 012316 (2006).
[61] Q.-M. Ding, X.-X. Fang, X. Yuan, T. Zhang, and H. Lu, Phys. Rev. Research **3**, 023228 (2021).
[62] C. Kokail, C. Maier, R. van Bijnen, T. Brydges, M. K. Joshi, P. Jurcevic, C. A. Muschik, P. Silvi, R. Blatt, C. F. Roos *et al.*, Nature (London) **569**, 355 (2019).
[63] K. Kowalski and B. Peng, J. Chem. Phys. **153**, 201102 (2020).
[64] H. J. Vallury, M. A. Jones, C. D. Hill, and L. C. L. Hollenberg, Quantum **4**, 373 (2020).
[65] R. Horodecki, P. Horodecki, M. Horodecki, and K. Horodecki, Rev. Mod. Phys. **81**, 865 (2009).
[66] T. Brydges, A. Elben, P. Jurcevic, B. Vermersch, C. Maier, B. P. Lanyon, P. Zoller, R. Blatt, and C. F. Roos, Science **364**, 260 (2019).
[67] W. Hoeffding, Ann. Math. Stat. **19**, 293 (1948).
[68] H. R. Grimsley, S. E. Economou, E. Barnes, and N. J. Mayhall, Nat. Commun. **10**, 3007 (2019).
[69] H. L. Tang, V. Shkolnikov, G. S. Barron, H. R. Grimsley, N. J. Mayhall, E. Barnes, and S. E. Economou, PRX Quantum **2**, 020310 (2021).
[70] Z.-J. Zhang, J. Sun, X. Yuan, and M.-H. Yung, arXiv:2011.05283.
[71] S. Bravyi, S. Sheldon, A. Kandala, D. C. Mckay, and J. M. Gambetta, Phys. Rev. A **103**, 042605 (2021).
[72] D. Su, R. Israel, K. Sharma, H. Qi, I. Dhand, and K. Brádler, Quantum **5**, 452 (2021).
[73] Y. Li and S. C. Benjamin, Phys. Rev. X **7**, 021050 (2017).
[74] K. Temme, S. Bravyi, and J. M. Gambetta, Phys. Rev. Lett. **119**, 180509 (2017).
[75] J. R. McClean, Z. Jiang, N. C. Rubin, R. Babbush, and H. Neven, Nat. Commun. **11**, 636 (2020).
[76] J. Sun, X. Yuan, T. Tsunoda, V. Vedral, S. C. Benjamin, and S. Endo, Phys. Rev. Applied **15**, 034026 (2021).